EUROPEAN ORGANIZATION FOR NUCLEAR RESEARCH

# A study of the transverse fluctuations of hadronic showers in the NOMAD electromagnetic calorimeter

D. Autiero[1]  M. Baldo-Ceolin[2]  F. Bobisut[2]  L. Camilleri[1]  P.W. Cattaneo[3]  V. Cavasinni[4]
D. Collazuol[2]  G. Conforto[5]  C. Conta[3]  M. Contalbrigo[2]  A. De Santo[4]  L. Di Lella[1]
R. Ferrari[3]  V. Flaminio[4]  M. Fraternali[3]  D. Gibin[2]  S.N. Gninenko[6]  G. Graziani[7]
A. Guglielmi[2]  E. Iacopini[7]  M.M. Kirsanov[5,9]  A.V. Kovzelev[6]  S. Lacaprara[2]  A. Lanza[3]
L. La Rotonda[8]  M. Laveder[2]  A. Lupi[7]  A. Marchionni[7]  F. Martelli[5]  M. Mezzetto[2]
D. Orestano[3,10]  F. Pastore[3,10]  E. Pennacchio[5]  R. Petti[3]  G. Polesello[3]  G. Renzoni[4]
C. Roda[4]  A. Rubbia[1]  F. Salvatore[3]  A. Sconza[2]  A.N. Toropin[6]  M. Valdata-Nappi[8]
M. Veltri[5]  V. Vercesi[3]  S.A. Volkov[6]

## Abstract

The transverse shower shape of the energy deposition of hadrons in the NOMAD lead glass calorimeter has been studied by exposing a prototype of this calorimeter to pion test beams of various momenta and incident angles. Large event to event fluctuations in the shower shape and significant energy depositions far from the incident hadron were observed making it difficult to associate all the deposited energy to the incident hadron that caused it. Since in the NOMAD detector the momenta of charged hadrons are measured by a magnetic spectrometer, such an association is necessary to be able to subtract from the calorimeter all the energy caused by the observed charged hadrons in order to avoid double counting. Probability functions based on the measurements have been developed to describe fluctuations of the lateral shower shape. Starting from these functions, an algorithm is developed for identifying the energy deposition associated to a charged hadron. The identification and separation of overlapping showers based on these functions is also discussed. The Monte Carlo simulation of the calorimeter reproduces the test beam data well therefore allowing the application of the algorithm at angles and momenta not studied in the test beam.

*Submitted to Nucl. Instrum. Methods  Phys. Res. A*

[1] CERN, Geneva, Switzerland
[2] Univ. of Padova and INFN, Padova, Italy
[3] Univ. of Pavia and INFN, Pavia, Italy
[4] Univ. of Pisa and INFN, Pisa, Italy
[5] Univ. of Urbino, Urbino, and INFN Florence, Italy
[6] Inst. Nucl. Research, INR Moscow, Russia
[7] Univ. of Florence and INFN, Florence, Italy
[8] Univ. of Calabria and INFN, Cosenza, Italy
[9] Now at INR, Moscow, Russia
[10] Now at Roma-III Univ., Rome, Italy

# 1    Introduction

The aim of the NOMAD experiment at the CERN SPS wide-band neutrino beam is to search for $\nu_\mu$ to $\nu_\tau$ oscillations in a predominantly $\nu_\mu$ beam with higher sensitivity than previously achieved[1]. The experiment intends to observe $\nu_\tau$'s through their charged current interactions. The produced $\tau$'s are identified through their decays using only kinematical criteria applied to the transverse momenta of the hadronic jets and of leptons produced in the final state of neutrino interactions.

The NOMAD detector is described in detail in ref.[2]. Here only its main features will be briefly mentioned. A sketch of the NOMAD detector is shown in figure 1.

The active target consists of 132 planes of drift chambers located in a magnetic field of 0.4 $T$ which allows the determination of the momenta of the charged particles. The target is followed by a transition radiation detector (TRD) to enhance $e/\pi$ separation and by a lead-glass electromagnetic calorimeter (ECAL) with an upstream preshower detector (PRS). The design, construction and performance of the ECAL were presented in ref. [3]. The trigger is provided by two planes of scintillation counters $T_1$, $T_2$. A veto in front of the magnet rejects upstream neutrino interactions and muons incident on the detector. A hadronic calorimeter and a muon spectrometer placed outside the magnet provide an estimate of the energy of the hadronic component in the event and the muon identification respectively.

For each neutrino event the full hadronic jet momentum is reconstructed as a sum of the momenta of the charged tracks as measured in the drift chambers and of the momenta of the photons whose energies are measured in the ECAL. Since the momenta of charged hadrons are measured by the magnetic spectrometer their energy deposition must be identified and subtracted from the total energy in the calorimeter in order to avoid double counting. The rest of the ECAL energy is assigned to the neutrals, and hence the energy due to charged hadrons, that remains in the calorimeter after the subtraction procedure must be minimized while keeping the efficiency for real photon detection as high as possible. The identification of the hadronic energy in the ECAL is based upon the the lateral shape of the energy deposition with respect to the trajectory of the charged track. The shape of the energy deposited depends on the particle type, its energy , angle of incidence and impact point at the front surface of the ECAL. To develop a subtraction algorithm the response of the calorimeter to hadrons showering in the lead glass must therefore be well known.

In this paper test beam results and a Monte Carlo simulation of the response of an ECAL prototype to negative pions in the energy range from 5 to 15 GeV are presented.

It was found that due to the large event-to-event fluctuations of the lateral shape of the energy deposited by a charged hadron in the calorimeter an association of *all* this energy to the incoming track is a difficult problem. In particular, rare hadronic events with energy deposition at distances from the incident position much larger then the ECAL cell size ( $\approx 10cm$) have been observed both in the test beam and Monte Carlo data. An example of such an event initiated by a single 5 GeV pion in the ECAL is shown in figure 2, where one can see that to account for more than 90% of the total pion energy, cells as far as 40 cm must be included. In real neutrino events this energy could be misidentified and counted as neutral. Such phenomena initiated by single hadrons will be quite rare in the NOMAD detector. Nevertheless, taking into account the expected sensitivity of the experiment [1], the energy spectra of secondary hadrons and their multiplicity , such events could be expected to occur with a probability $\approx 10^{-5}$ and could possibly result in a source of background in NOMAD . To estimate this background, data on the average
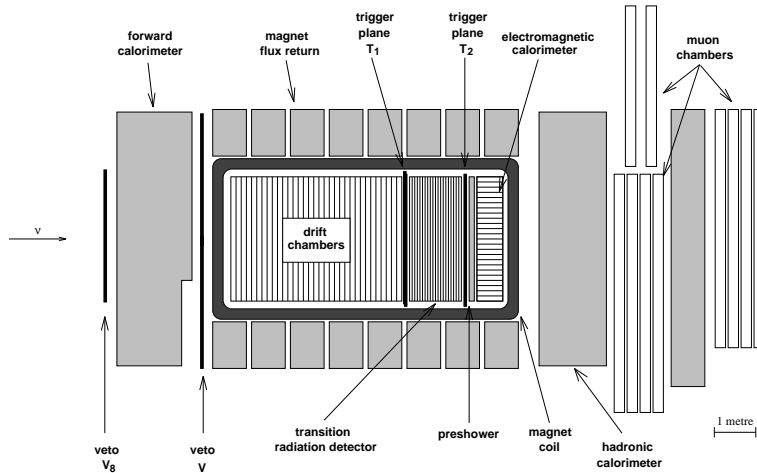
Figure 1: *Side view of the NOMAD detector.*

properties of hadronic showers in the lead-glass are not sufficient. The knowledge of event-by-event fluctuations of the lateral shape of the energy deposited by charged hadrons in the calorimeter is also needed.

The average lateral shape of hadronic showers has been recently examined by several groups in different types of calorimeters at energies up to 150 GeV. The data cover nearly five decades in the average lateral energy deposit; for example see [4], and references therein.

In this paper we have studied the fluctuations of the lateral hadronic shower shape. A phenomenological method to describe event-by-event fluctuations of the lateral shape of a hadronic shower in terms of probability functions has been developed. We discuss the performance of the method to identify isolated or overlapping hadronic showers as well as overlapping hadronic and electromagnetic showers. The method is also useful to estimate the probability that the energy remaining in the calorimeter after subtraction of the charged hadron component be assigned to fake neutral showers.

The paper is organized as follows. The calorimeter prototype and the test beam setup are described in section 2. The description of the method used to measure accurately the response of ECAL to hadrons is given in section 3. Section 4 describes the Monte Carlo simulation used to reproduce the hadronic showers in the calorimeter. In sections 5 and 6 the data and the analysis method are discussed. A description of the shower fluctuations and a MC comparison is also shown in section 6. The results on identification and subtraction of the energy deposited by isolated and overlapping showers are presented in sections 7 and 8 respectively. The effect of angle and energy dependence in the model developed is discussed in section 9. Conclusions are given in section 10.

## 2     Experimental setup

The data presented below were obtained by exposing an ECAL prototype, consisting of 5x11 lead glass modules, to the CERN SPS X5 test beam, using negative electron, muon and pion beams with momenta from 5 to 15 GeV/c. A sketch of the X5 test beam setup is shown in figure 3.

The ECAL prototype was placed on a movable table so that it could be displaced in the horizontal and the vertical directions through the beam. Prototype modules are made of TF1-000 lead glass. They each have a thickness of 19 radiation lengths ($\sim 50\,cm$ )
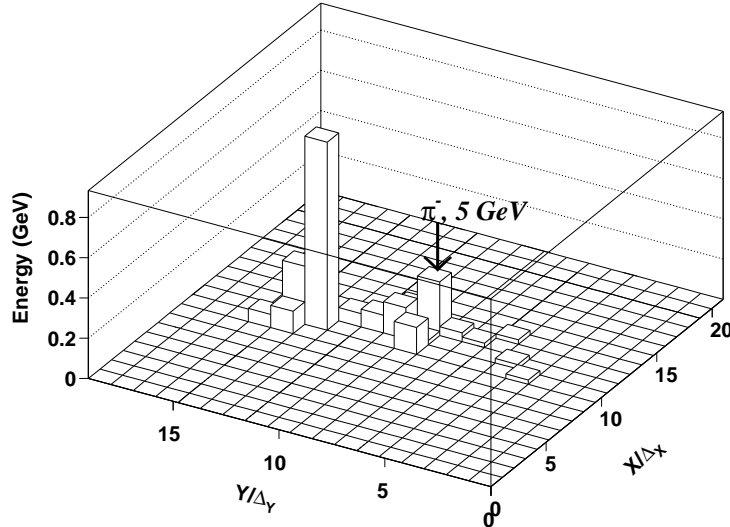
2

Figure 2: *Monte Carlo example of a hadronic event with rare topology of the energy deposited in the calorimeter by 5 GeV negative $\pi$ entering ECAL at the point marked by the arrow. The calorimeter cell size is equal to $\Delta_x = 79mm$ and $\Delta_y = 112$ mm in the x and y directions respectively.*

and a rectangular cross section of $7.9 \times 11.2 \ cm^2$. The radiation length $X_0$ has been calculated to be 2.78 cm and the nuclear interaction length $\lambda \approx 46 \ cm$, i.e. the length of a module corresponds to 1.1 $\lambda$. Each module was viewed by a two stage photo-multiplier ( Hamamatsu R2186 tetrode) designed to operate in intense magnetic fields and placed at $45^0$ with respect to the axis of the block and to the magnetic field direction to reduce the loss of gain caused by the magnetic field. Tetrodes were read out by 12 bit peak sensitive ADCs. The energy calibration was performed by irradiating the center of each module with 10 GeV electrons. The beam trigger was defined by three scintillator counters, $10 \times 10 \times 0.5 \ cm^3$, and a veto counter covered the full ECAL prototype surface with a $7 \times 10 \ cm^2$ hole in the center. The resulting $\pi^-$ beam was slightly defocused in order to irradiate the ECAL cell uniformly. The maximum trigger rate was about 300 events per 2 sec SPS spill at 15 GeV. The beam divergence was kept to less than 10 $mrad$. The x and y coordinates of the incoming particles were measured by a delay wire chamber with 200 $\mu m$ space resolution, placed approximately 1 meter upstream of the calorimeter. In order to prevent charge pile-up in the amplifier chain, events were rejected if a second particle arrived within 20 $\mu s$ before and 2 $\mu s$ after the trigger. During the run periods the stability of the tetrode gain, the electronics and the pedestals were regularly checked.

Note that, although in the NOMAD detector the calorimeter is placed inside the magnetic field of 0.4 $T$ the test beam data were taken without a magnetic field. The effect of the field on fluctuations of the lateral shape of hadronic showers is estimated to be negligible.

## 3    Background measurement

The measurements of the lateral hadronic shower fluctuations at the required level of precision could be affected by a contribution of background from the beam halo. This background could come from the secondary interactions of the pions in the upstream
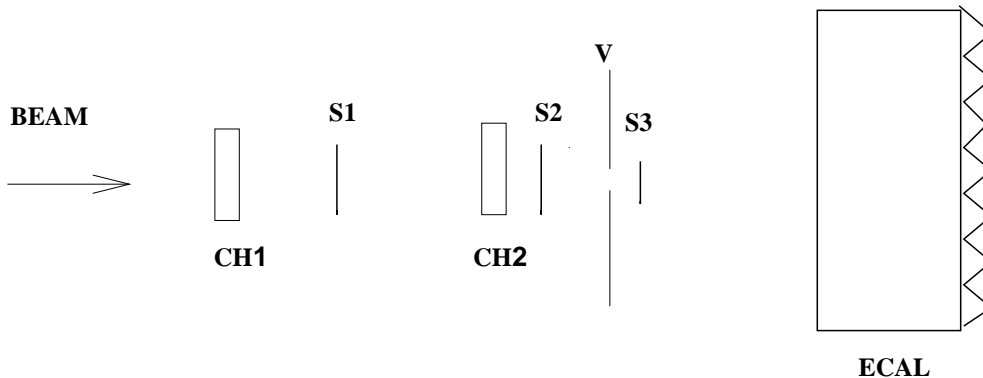
Figure 3: *Test beam setup. $S_1$, $S_2$, $S_3$ are trigger counters, $CH_1$, $CH_2$ are the beam-monitor delay wire chambers, V is the veto wall, ECAL is the matrix of lead-glass blocks.*

beam material such as scintillator counters, windows of the beam pipes , air, etc.. and also from the beam particles decaying in flight.

The amount of halo background in the hadronic sample was evaluated as follows. For each pion momentum two measurements at the same beam and trigger conditions were performed. In the first, the data run, the response of the ECAL to pions was measured as described in Sec.2. In the second measurement, the halo run, the central block of the calorimeter prototype, corresponding to the beam impact position, was moved downstream by approximately 0.5 m in order to avoid pion interactions inside the ECAL fiducial volume. In this case the energy deposition in the ECAL came mainly from the beam halo particles.

Since the contribution of the lateral leakage from the central block to the surrounding blocks from halo particles entering the central block was excluded the measured halo background was underestimated. Since our purpose was to estimate the level of this background at radii larger than ECAL cell size, the systematic error from this effect was found to be small.

Data were normalized to the number of entering pions in each run. After this normalization the halo run distributions were subtracted from the corresponding data run distributions resulting in corrected distributions. The procedure assumes that beam and measurement conditions are stable during these two runs. The stability of these conditions, in particular of the efficiency of the veto wall, was regularly checked.

## 4    Monte Carlo simulation

In order to understand the hadronic response of the lead-glass, a full GEANT (version 3.214) simulation was performed, taking into account the Cerenkov light propagation and the FLUKA package for hadronic interactions [6]. A high statistics sample ($\sim 100k$ events) was generated in test-beam conditions as a function of the incidence angle ($\theta = 0^0$, $10^0$, $15^0$, $20^0$ ) and energy ($E = 2, 5, 10, 15 GeV$). The above statistics was found to be a good compromise between the computation time needed for simulations and the required sensitivity level (section 1).

A simulation was needed to analyze kinematical configurations not directly available in real data. In particular the angular dependence was studied since this effect might introduce deviations from the parameterized probability distributions (evaluated at $\theta = 0^0$) and a broad spectrum is expected in NOMAD for charged hadrons. Moreover no experimental data could be taken in the low energy region ($E < 5 \; GeV$), where the

4

probability to have energy deposits at large distances from the impact point is expected to increase.

The distributions for the available test beam measurements were compared to the corresponding Monte Carlo ones to test the global reliability of the simulation. The purpose of such a comparison was to check if lateral hadronic shower fluctuations were satisfactorily reproduced in the simulation from the point of view of the subtraction procedure. On the other hand rare processes with a large fraction of the particle energy deposited far away from the impact point were observed in real data (section 1). Due to the experimental background level, the Monte Carlo simulation is the way to estimate their probability and to understand the physical processes that could cause such events. In particular a consistency check was needed for experimental data at low probability levels ($\leq 10^{-4}$), which could in principle be affected both by background contamination and systematic uncertainties, like geometrical acceptance effects (section 6).

Finally, as a further motivation, a simulation is needed to test the clusterisation algorithm based on the described model for hadronic showers.
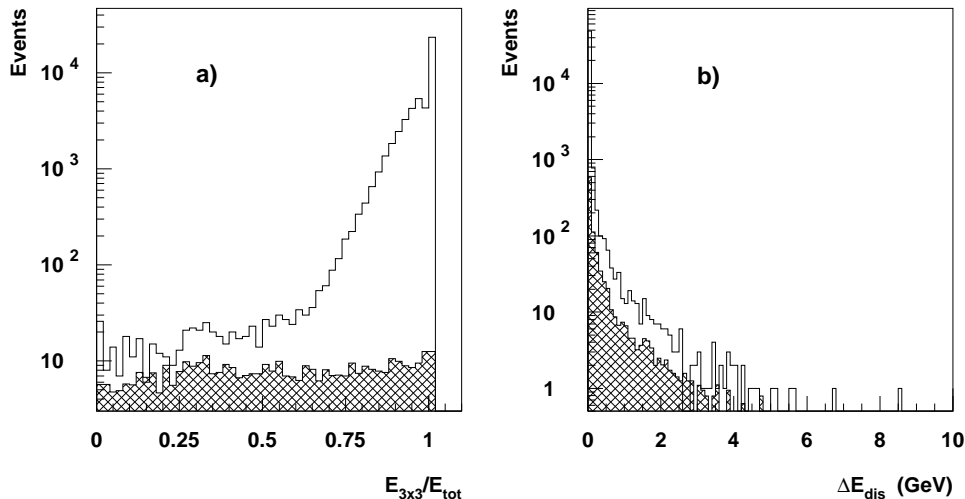


Figure 4: a) Distribution of fractional energy $E_{3\times3}/E_{tot}$ deposited by charged 15 GeV pions in the 3×3 cell cluster, where $E_{tot}$ is the total energy deposit in the ECAL. b) Distribution of total energy $\Delta E_{dis}$ deposited by charged 15 GeV pions in the cells disconnected from the main cluster, i.e. the cluster hit by the incoming hadron. The same distributions obtained in background measurements are also shown as hatched areas.

## 5    Data sample and cluster analysis

During the 1995 and 1996 run periods data were taken with negative electron, muon, and pion beams of 5,6,8,10,15 GeV/c at normal incidence on the calorimeter. The electron data were used for calibration of the ECAL prototype. While muon data were used to estimate and subtract from the pion sample the muon contamination, which is due to $\pi$ and $K$ decays upstream of the detector. The average number of events recorded for each run was about $10^5$. For 5 and 15 GeV/c data were also recorded at $10^0$ angle of incidence . To select samples of single hadronic showers only events with a single track in

the beam chambers were accepted. This requirement helps to exclude some fraction of the hadrons which start showering upstream of the calorimeter. Such events are characterized by a large hadronic shower in the ECAL prototype. The efficiency of the VETO wall was about 97% , thus not all halo events were rejected. The effect of the surviving halo events was taken into account as described in section 3.

The analysis of the data was based on a cluster algorithm described below. As the RMS of the pedestal distribution was 0.5 channels, only cells with an ADC value of at least 2 channels ($\approx 50$ MeV) or more were considered. Groups of *connected* cells that touched each other are called clusters. The cluster that is entered by the incoming charged hadron is called the *main* cluster.

The results obtained from test beam studies of electrons show that due to the short radiation length $X_0$ of the lead glass e-m clusters are compact objects and have a lateral size roughly equal to the lateral size of one ECAL module. On average an electron impinging on the calorimeter at angles of incidence less than $10^0$ deposits more than 99% of its energy in a 3×3 cluster.

Hadronic showers have large variations in the amount of deposited energy. This can range from $\approx 0.5\ GeV$ which is the typical energy deposited in the calorimeter by a pion traversing it without interacting, to the full energy of the particle which happens when the pion charge exchanges early in the lead glass.

The lateral size and its fluctuations for hadronic showers are also significantly larger than for electromagnetic ones. For example, 95 % of the full hadron shower energy is contained in a cylinder of radius $R \approx 1\lambda$, where $\lambda$ is the nuclear interaction length in matter. The mean free path of hadrons in the lead glass ( $\approx 50\ cm$ for charged pions) is larger than the size of a lead glass cell therefore hadronic secondaries scattered at large angles can travel large distances before interacting. This can result in significant signals in cells far from the hadron impact point and even *disconnected* from the main cluster as test beam data shows. The use of the clustering algorithm for such hadronic events may produce a number of clusters which are not easily associated to the primary track and may be considered as hits due to a different particle entering ECAL. Figure 3 shows an example of energy deposition in the calorimeter by a 5 GeV pion where the problem of associating all the energy deposition to the incoming track is evident. The problem is also illustrated in figure 4a which shows the distribution of fractional energy $E_{3\times3}/E_{tot}$ defined as the ratio of the energy deposited by 15 GeV pions in the 3×3 cell cluster centered on the incoming hadron to the total energy deposit in the ECAL. A tail towards low values can be seen. The distribution of total energy deposited in disconnected cells is shown in figure 4b. Approximately 10% of the events have more than one cluster, i.e. at least one disconnected cell.

In principle, the algorithm to remove hadronic energy from the calorimeter could be simply based on the subtraction of energy deposited in the 3×3 cluster or main cluster that is associated to the incoming track. However, although the average fraction of energy deposited inside these clusters is about 90% , the fluctuations of the energy deposited outside of this cluster could be up to a few GeV as seen from figure 4. Since this residual energy could be deposited at different radii, the algorithm should also provide an estimate of the probability for any cell in the ECAL with nonzero energy deposition to be produced by the given incoming track. Our attempt to build such tools is described below.
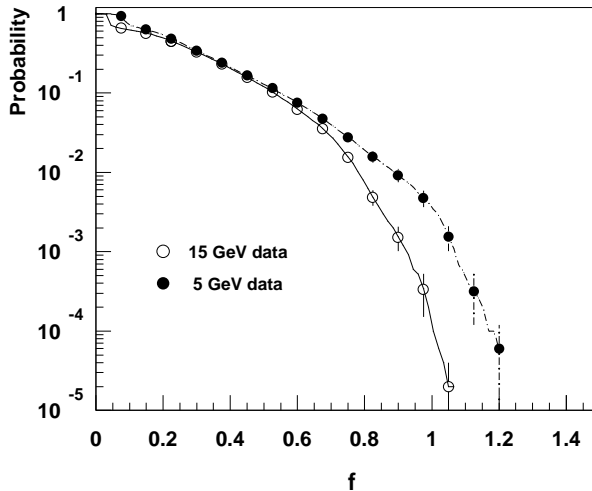
6

Figure 5: *The probability for 5 and 15 GeV pions to deposit, in a 2×2 cluster, an energy greater than a fraction $f$ of the beam energy.*

## 6     Probability functions and profiles for Isolated hadrons

It is important to note that in the test beam measurements the lateral cross section of the active part of the calorimeter prototype allows to detect energy deposited at radii $R$ up to $\approx 60\ cm$. However, the detection efficiency was not uniform in azimuth because the ECAL prototype has a rectangular shape (section 2). Corrections to the detection efficiency as a function of $R$ were then required. Our approach was first to compare test-beam results with Monte Carlo predictions for the given ECAL prototype. This procedure was intended to check the global reliability of the simulation and also to exclude large systematics in the measurement and analysis method. In particular this is a crucial point in order to study hadronic fluctuations at probability levels low enough to be affected by background. The MC simulation was then used to estimate the detection efficiency and to extend the analysis to the full NOMAD calorimeter.

The algorithm to identify and remove hadronic energy in the ECAL is based on reference hadronic shower profiles and probability functions for isolated hadrons[5]. These are defined in the following way:

  – the reference profile $A(f, R)$ predicts the average fraction of the hadron energy deposited in a cell located at a distance $R$ from the impact point of a hadron. The profile $A(f, R)$ is a function of the fraction $f$ of the total hadron energy deposited in the ECAL as defined below.
  – the probability function $P(\varepsilon, f, R)$ predicts the probability for an energy deposition in any ECAL cell to be greater than a given fraction $\varepsilon$ of the total energy of the incoming charged hadron. These functions are used to describe fluctuations of the lateral shape. Note that both $A(f, R)$ and $P(\varepsilon, f, R)$ vary with $f$.

The asymmetric cell shape and the large cell size, which is commensurate with the transverse radius of hadronic showers, will affect a description of the shower development simply based on global distances $R$. On the other hand, a two-dimensional parameterization in the plane $(x, y)$, which in principle could partially solve such problems, is more complex and very sensitive to the impact angles. The model described, based on the
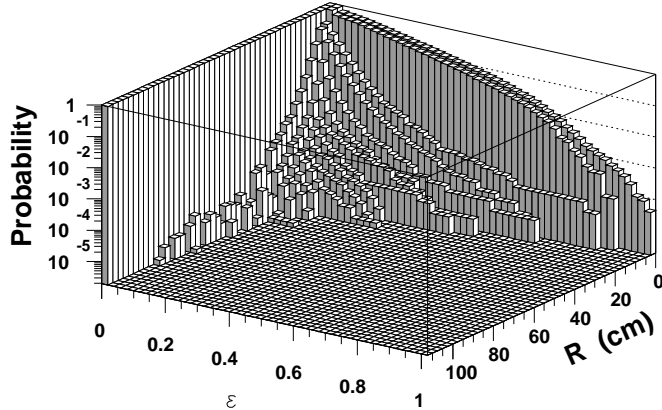
7

Figure 6: *Example of the two-dimensional probability distribution $P(\varepsilon, R)$ (averaged over all f values) to find an energy deposition greater than a given fraction $\varepsilon$ of the total pion energy in a cell at a distance $R$ from the impact point. The data refer to a pion energy of 15 GeV.*

$A(f, R)$ and $P(\varepsilon, f, R)$ functions, was found to be adequate for our purposes.

In order to determine a set of functions $A(f, R)$ and $P(\varepsilon, f, R)$, the test beam data were analyzed in the following way:

- the lead-glass cell to which the hadronic track extrapolates using the beam chamber information (hit cell) was identified.
- a 3×3 cluster was built around this cell.
- the energy depositions in the four possible 2×2 modules combinations of cluster cells that contain the central cell were calculated.
- the ratio $f = E_{2\times2}^{max}/P_{beam}$, where $P_{beam}$ is the incident hadron momentum and $E_{2\times2}^{max}$ is the largest 2×2 module energy of the four possible combinations, was calculated. It was also taken as a measure of the fraction of hadronic energy deposited in the ECAL. A 2×2 cell combination was chosen to minimize overlapping effects from close showers in $\nu$-events while estimating the fraction of hadron energy deposited in the ECAL with enough precision.
- the probability to deposit more energy in the 2×2 cluster than a given fraction $f$ was parameterized as a function of $f$. This probability was used to identify overlapping showers in $\nu$-events, when the energy deposited in the 2×2 cluster is greater than the track momentum. An example of this function is shown in figure 5.
- the test beam events were subdivided into 5 intervals of $f$ starting from 0 in steps of 0.2; the last interval included all values above 0.8.
- the distributions $N(\varepsilon, f, R)$ of the fractional energy $\varepsilon$ were built for each value of $R$ and for each of the 5 intervals of $f$.
- the probability to observe a fractional energy greater than $\varepsilon$ at a given $f$ and $R$, $P(\varepsilon, f, R)$ was obtained from the $N(\varepsilon, f, R)$ distributions by summing all the bins at a given $f$ and $R$ with fractional energy greater then $\varepsilon$ and normalizing the sum to the total number of events.

8

– the average $\varepsilon$ at a given $f$ and $R$, $A(f, R)$ was also obtained from the $N(\varepsilon, f, R)$ distributions.

The final probability functions were extracted from the data obtained by subtracting the spectrum obtained during the halo run from the spectrum obtained during the corresponding data run. An example of $P(\varepsilon, f, R)$ is shown in figure 6.

The distributions $P(\varepsilon, f, R)$ have smooth exponential shapes (figure 6). These functions were parameterized using the program MUDIFI (Multi Dimensional Fit, CERN library) as a sum of Chebyshev polynomials with maximum degree of 9.

The probability distributions $P(\varepsilon > 0.1, R)$ averaged over all $f$ values for $\theta = 0$ for data and for background runs is shown in figures 7a and 7c for 15 and 6 GeV/c pions respectively. The resulting background subtracted distributions are compared to the simulated distributions in figures 7b and 7d. An event selection was performed to obtain the integral distributions shown, keeping only particles impinging at a distance $\mid x \mid < \Delta_x/4$ and $\mid y \mid < \Delta_y/4$ from the center of the cell, $\Delta_x$ and $\Delta_y$ being the dimensions of the lead glass block. The general shape is well reproduced and the overall agreement is satisfactory at the level of the available statistics. The presence of the shoulder at low $R$ values, is due to the effect of the cell size in this region. This effect is well reproduced in the Monte Carlo.

The total longitudinal depth of the NOMAD calorimeter is approximately equivalent to $\lambda$, so that the probability for charged hadrons to interact within the lead-glass is less than 1. As a consequence the hadronic shower is expected to be less collimated along the track direction for lower impact energies and the probability for the particle to scatter at large angles is enhanced correspondingly. The energy distribution may then extend to larger transverse distances from the impact point as shown in figure 7d for $E = 6\ GeV$, where a tail is visible for $R > 20\ cm$. In such conditions the geometrical acceptance of the experimental prototype begins to affect the above distribution. The MC predictions correctly describe the experimental behavior of the prototype and can therefore be used to correct for acceptance inefficiencies and compute the distributions for the full calorimeter. It should be noted that a prototype greater than $1\ m$ in diameter is needed to study fully hadronic fluctuations at the level $\leq 10^{-5}$. At higher energies the prototype size was adequate and no tail was observed (figure 7b).

To evaluate the quality of this parameterization in describing of individual hadronic showers several variables were studied. The best results were obtained with a variable $\Psi$ defined as [4]:

$$\Psi = \sum_{ij} \frac{R_{ij} \times \left( E_{ij}^{exp} - E_{ij}^{pred} \right)^2}{E_{beam}^2} \qquad (1)$$

where the sum extends over all connected cells in the main cluster, $R_{ij}$ – is the distance between the impact point and the cell $(i, j)$, $E_{ij}^{exp}$ – is the experimental energy deposition in the cell $(i, j)$, $E_{ij}^{pred}$ – is the energy deposition predicted by the parametrized reference profile in the cell $(i, j)$, and $E_{beam}$ - is the beam energy. This variable emphasizes energy depositions at large radii, which is the region of interest in this study.

The distributions of $\Psi$ values for 5 and 15 $GeV$ single pions at $\theta = 0^0$ are shown in figure 8a-b. They are sharply peaked at zero demonstrating that the data are described correctly. The cut $\Psi < 0.5$ retains 95% of single pion events. The same algorithm previously described for test-beam data was applied to Monte Carlo samples. The calculated $\Psi$ distributions, also shown in figure 8a-b, indicate a similar behavior of hadronic showers in real data and simulated events.
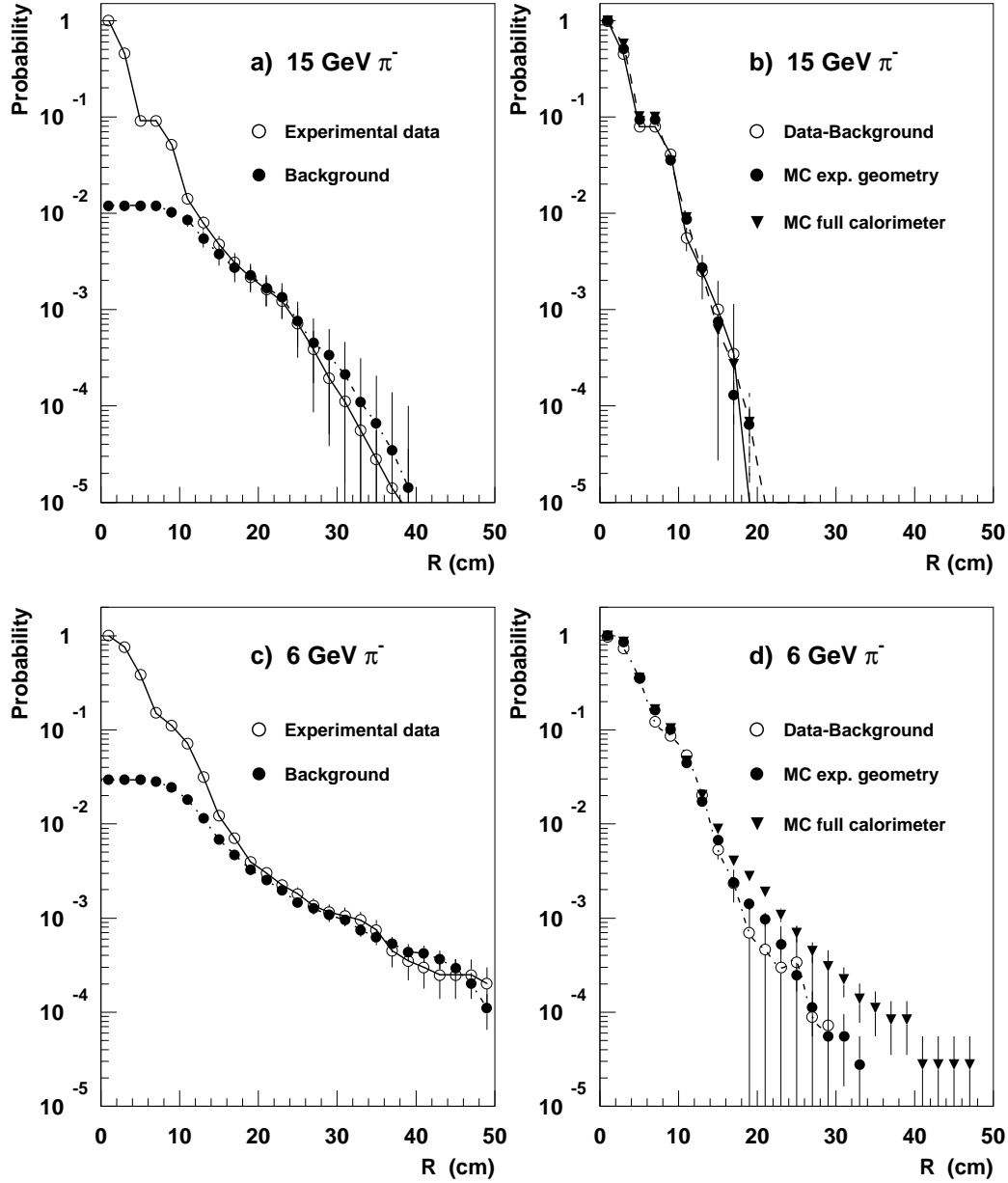
Figure 7: *The probability functions* $P(\varepsilon > 0.1, R)$ *(averaged over all f values) for 6 GeV and 15 GeV* $\pi^-$ *entering the central part of the cell: a)-c) for data and beam halo background measurements; b)-d) for experimental data after halo background subtraction and for MC simulations of the experimental prototype and of the full calorimeter size. The curves are a polynomial fit to the data.*
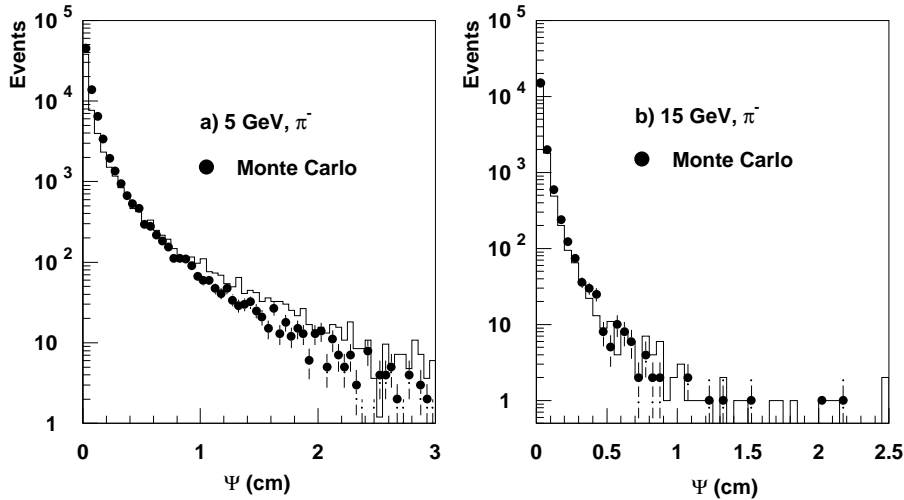
Figure 8: $\Psi$ distributions for showers initiated by a) 5 GeV and b) 15 GeV $\pi^-$ at $\theta = 0^0$ (averaged over all f values). The corresponding Monte Carlo distributions are shown for comparison.

## 7 Subtraction of energy deposited by isolated hadrons

### 7.1 Algorithm

The functions $A(f, R)$ and $P(\varepsilon, f, R)$ as defined can then be used to estimate the energy to be subtracted from the observed calorimeter energy for single isolated hadrons.

Isolated hadrons are identified as events with one incoming charged track into the ECAL prototype. These single shower candidates were analyzed as follows:

- the minimum probability level $P$ for a cell to be included is decided upon. The lower the acceptable probability level the less energy belonging to the hadron will be lost but the more superfluous energy will be associated to it. The probability levels used below were chosen purely as an example. For the analysis of real neutrino data the value of $P$ must be tuned.
- the ratio $f$ for each track, computed as described in section 5, was used to chose reference hadronic shower profiles and probability functions for the description of a given cluster shape.
- if $f \leq f(P)$, as obtained from figure 5 the energies of the 4 cells from the 2×2 module were removed from the ECAL and used to form the subtracted hadronic cluster, the energies in these 4 cells being set to 0.
- if the energies deposited in the remaining cells of the cluster are less than those allowed by the minimum probability level these energies are added to the hadronic cluster, and the contents of the cells are set to 0. Otherwise, the average energy, predicted by the reference shower profile is subtracted, added to the hadronic cluster and the content of the cell is set to its original content minus this average energy.
- if $f > f(P)$ the procedure described in the last item is applied to all the cells of the cluster using the $A(f, R)$ and $P(\varepsilon, f, R)$ functions defined for $f > 0.8$.

The procedure results in a set of subtracted isolated hadronic clusters and a set of remaining cells, - the latter one candidates to be reconstructed as neutral energy clusters in the ECAL. It is important to note that the algorithm provides also for each remaining
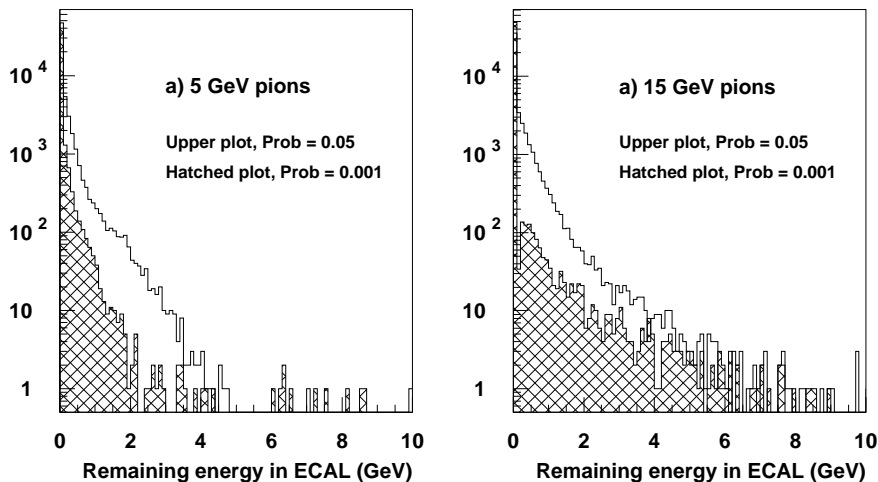
11

Figure 9: *Distributions of the remaining energy in the calorimeter, after subtraction of the estimated hadronic energy deposited by a) 5 GeV and b) 15 GeV $\pi^-$ at probability levels $P = 0.05$ (solid plots) and $P = 0.001$ (hatched plots).*

cell, close to a hadron the probability for it to be caused by this hadron. Later this can be taken into account in the analysis of real data.

## 7.2 Results for isolated hadronic showers

The algorithm was tested for 5 and 15 GeV isolated pions. The probability that the measured calorimetric energy in a cell originates from the given hadronic shower was required to exceed values that varied from $P$=0.1 to $P$=0.001. For example, after the subtraction procedure at a probability level $P$=0.05 the number of events which still have nonzero amplitudes (above $E_{thr} = 50$ MeV per cell) is $\simeq 30.2$ % for 5 and $\simeq 32.4$ % for 15 GeV pions. The distributions of energy remaining in the calorimeter for probability levels $P$=0.05 and $P$=0.001 are shown in figure 9. The average residual energy at $P$=0.05 is $\Delta E_{res}$=168 MeV and $\Delta E_{res}$=204 MeV for 5 and 15 GeV respectively.

The dependence of this average energy on the probability level is shown in figure 10a-b with the corresponding values obtained by applying the same subtraction procedure to MC data. The results for simulated events are compatible with the experimental values for a large range of probability levels. This allows the parameters of the algorithm to be tuned using MC simulations, in order to optimize both the reconstruction efficiency for photon identification and the rejection against fake neutral clusters.

## 8   Overlapped Hadronic Energy Subtraction

The above probability functions can be used to disentangle overlapping charged hadrons, a charged hadron overlapping a neutral hadron and a charged hadron overlapping a photon electromagnetic cluster. The algorithm must be optimized to get a good reconstruction efficiency for the neutral energy and also generate a minimum number of fake clusters. These two requirements are not always compatible and the final choice of probability level will depend on the particular physics analysis being performed.
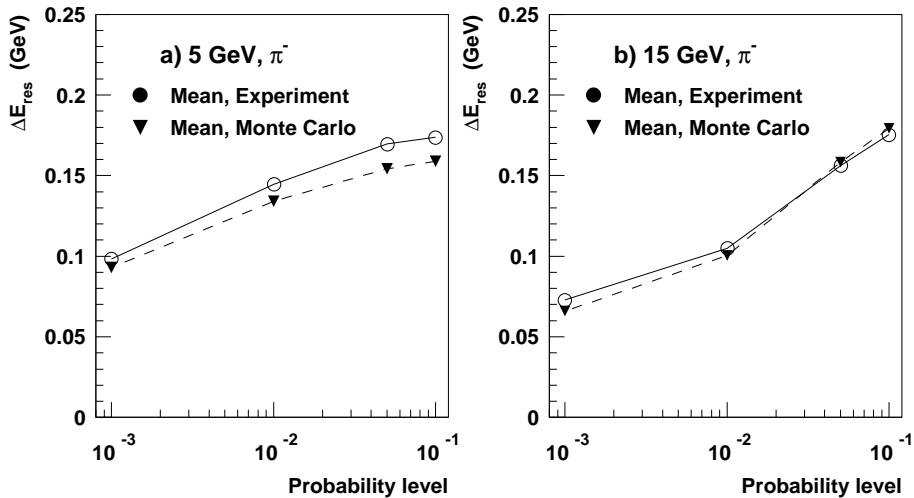
Figure 10: *Average values of the residual energy after hadron subtraction for a) 5 GeV and b) 15 GeV $\pi^-$ as a function of selected probability level P. The corresponding MC values are also shown.*

## 8.1 Overlapped charged hadrons

The algorithm described above is extended to overlapping charged hadrons as follows:

- tracks are matched with hit cells.
- the $f$ ratios are calculated as described above. However, if some particular cell used to calculate the 2×2 module energy belongs to a 2×2 module from another hadronic shower as well, its energy is divided between the overlapped hadrons in proportion to the energies deposited in the corresponding hit cells.
- the calculated ratios $f$ are used to choose the probability functions for the description of a given cluster energy configuration.
- for each cell (i,j) from the cluster the probability $P'_k(E_{ij})$ to observe a given amount of energy $E_{ij}$ is calculated for each hadron. If one of the hadrons has a probability in a particular cell greater than the selected level $P'$ the entire cell energy is associated to this hadron. If more than one hadron has a probability greater than $P'$, the cell energy is divided between them in proportion to the probabilities. Otherwise if no hadron contributes at a level $P'$, the maximum average predicted energy of the overlapped hadrons is subtracted and the remaining energy is associated to the cell to form the ECAL neutral energy.

## 8.2 A charged hadron overlapping a neutral hadron

The *charged $\pi$/neutral hadron* separation was simulated using the test beam data as follows. The showers from pions from two separate events and entering calorimeter at some relative distance were merged. One of the incoming pions was considered as a neutral hadron and therefore the knowledge of its impact point was not used. The position of the other one was assumed to be known. The $\Psi$ distribution for these overlapped events was calculated using as a reference profile the parameterization obtained from single hadron events. The resulting $\Psi$ distribution for two overlapped 5 GeV pions separated by 15 cm
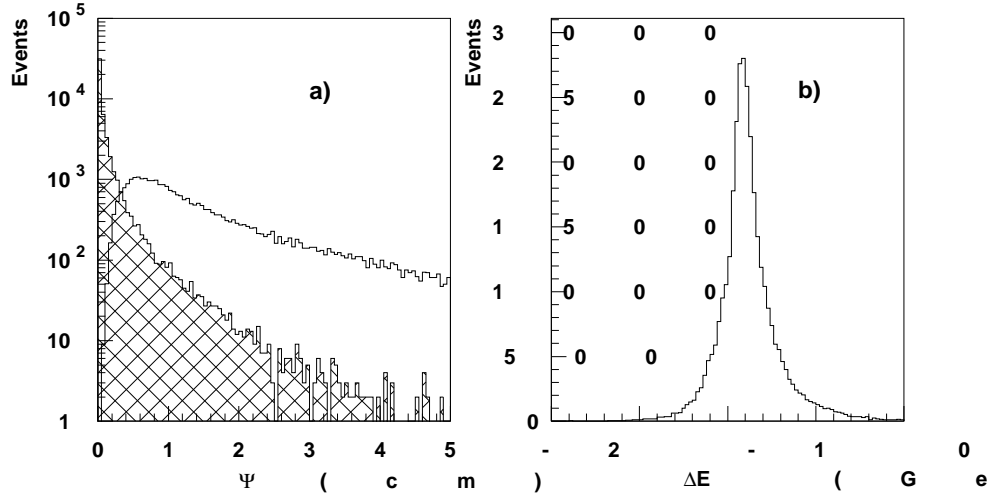
13

Figure 11: a) *Distribution of $\Psi$ values for 5 GeV $\pi$ + 5 GeV $\pi$ (considered as neutral hadron) overlapped at a relative distance $d \approx 15$ cm. The distribution of $\Psi$ values for single 5 GeV pions is shown for comparison (hatched part). b)The distribution of $\Delta E = E_{recon} - E_{real}$ described in the text for an overlapping neutral hadron.*
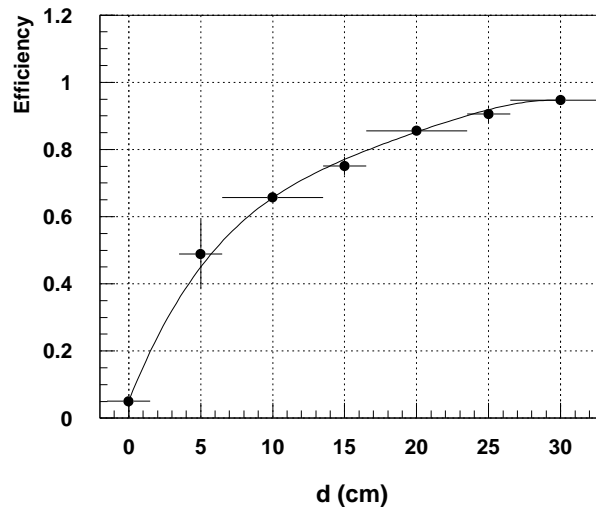


Figure 12: *The probability of identification a 5 GeV $\pi$+5 GeV $\pi$ pair as a function of their relative distance $d$ using the $\Psi$ criterion cut that retains 5% of the isolated pions. One of the pions is considered as a neutral hadron.*

14

on average, shown in figure 11 differs from the $\Psi$ distribution of single pions, also shown in the figure. The separation algorithm was applied to events with $\Psi > 0.5$ cm. As noted earlier only 5% of the single hadron showers survive this cut.

After subtraction of the first shower associated to the incoming charged track the remaining energy was examined to form a neutral cluster. For this purpose the program constructed a cluster around the cell having the largest amplitude from the remaining nonzero cells. This cluster was treated as the neutral shower. The efficiency to find this shower after subtraction of the charged pion energy deposit is in agreement with the one obtained with the $\Psi$ criterion. In figure 11b the distribution of the difference between the real and reconstructed neutral hadron energies is shown for a relative average distance $d$ of 15 cm between the particles. The probability of identification a $\pi + \pi$ pair as a function of their relative distance $d$ using the $\Psi$ criterion cut that retains only 5% of the isolated pions is shown in figure 12. One can see that a *charged $\pi$/neutral hadron* overlap can be identified as such in more than 75 % of the cases for $d \approx 15$ cm.

## 8.3  A charged hadron overlapping a photon

The algorithm could help to reduce the loss of photons due to their overlap with hadronic clusters and to identify the energies of the overlapped photons. Photon showers are narrow, so it could be expected that they would be better identified by the $\Psi$ criterion at a given distance from an incoming pion, than two overlapped hadrons.

The $\gamma/\pi$ separation was investigated in the same way as the overlap of two hadrons. Two real showers one from a pion and one from an electron (considered as a photon) entering the ECAL prototype at a relative average distance $d$ were merged. The resulting energy deposition shape was compared to the isolated pion shape using the $\Psi$ criterion ( figure 13a) and analyzed with the subtraction algorithm in order to reconstruct the energy of the overlapping photons.

In figure 13b the difference $\Delta E = E_{recon} - E_{real}$ between reconstructed and real energy deposition for photons randomly distributed in energy from 3 to 7 GeV at a relative distance $d$ of 10 and 20 cm from 15 GeV single pions are shown. We consider events with $\Psi < \Psi_{cut}(=0.5$ cm) to be isolated pions. The probability of identification a $\pi + \gamma$ pair as a function of their relative distance $d$ using the $\Psi$ criterion cut that retains 5% of the isolated pions is shown in figure 14. One can see that a *charged$\pi$/photon* overlap can be identified as such in 90% of the cases for $d$ greater than 10 cm.

## 9     Angle and energy dependence

For an incidence angle $\theta \neq 0^0$, in general the charged track crosses more than one block and as a consequence the probability to have a large energy fraction at large transverse distances from the impact point is enhanced. This fact may increase in principle the residual energy after the hadron subtraction procedure, introducing some additional background in the cluster reconstruction algorithms.

Since a reasonable overall agreement was found between test-beam measurements and simulations for normal incidence, the effect of the angular dependence in the hadron subtraction procedure was studied using Monte Carlo data. In figure 15 the resulting $\Psi$ distribution for $\theta = 10^0$ and $E = 5 GeV$, averaged over all $f$ values, is compared with the corresponding experimental data sample. The general qualitative agreement allows to extend the simulation to larger angles, for which some deviations from the parameterized behavior at $\theta = 0^0$ are expected.
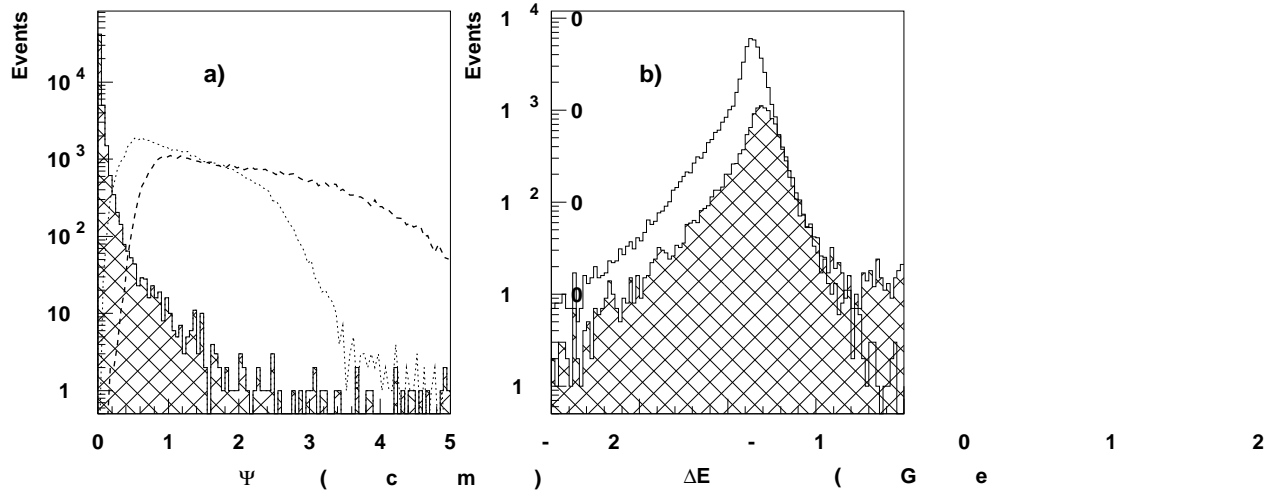
Figure 13: a) Distributions of $\Psi$ values for a 15 GeV $\pi$ overlapping 3÷7 GeV $\gamma$ at a relative distance $\approx$ 10 cm (dotted) and 20 cm (dashed). The distribution of $\Psi$ values for single 15 GeV pions is shown for comparison (hatched part). b) The difference $E_{recon}$-$E_{real}$ described in the text for photons overlapping with pion showers at a relative distance 10 cm (hatched part) and 20 cm.
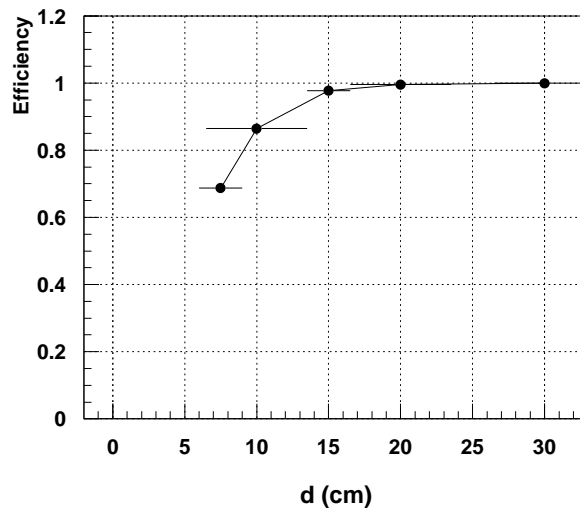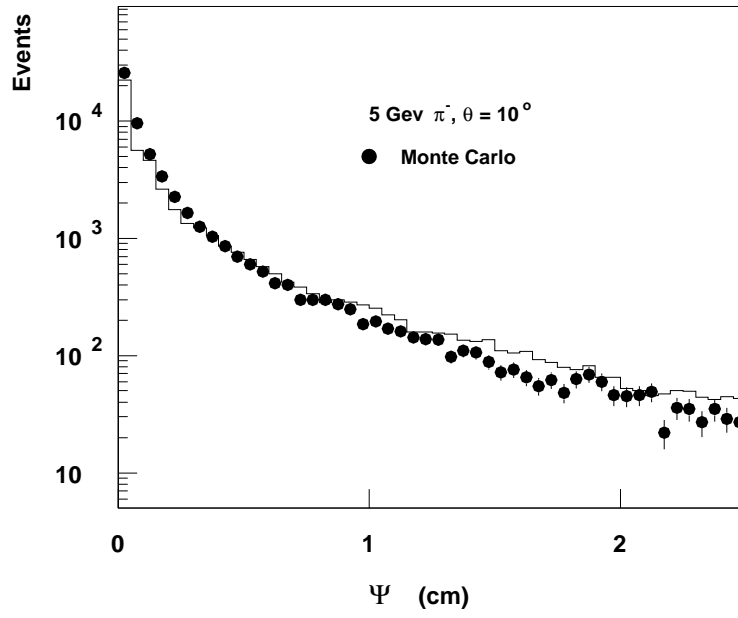


Figure 14: The probability of identification a 15 GeV $\pi$+ 3÷7 GeV $\gamma$ pair as a function of their relative distance $d$ using the $\Psi$ criterion cut that retains 5% of the isolated pions.

Figure 15: *Monte Carlo and experimental* $\Psi$ *distributions for 5 GeV* $\pi^-$ *for* $\theta = 10^0$ *(averaged over all f values).*
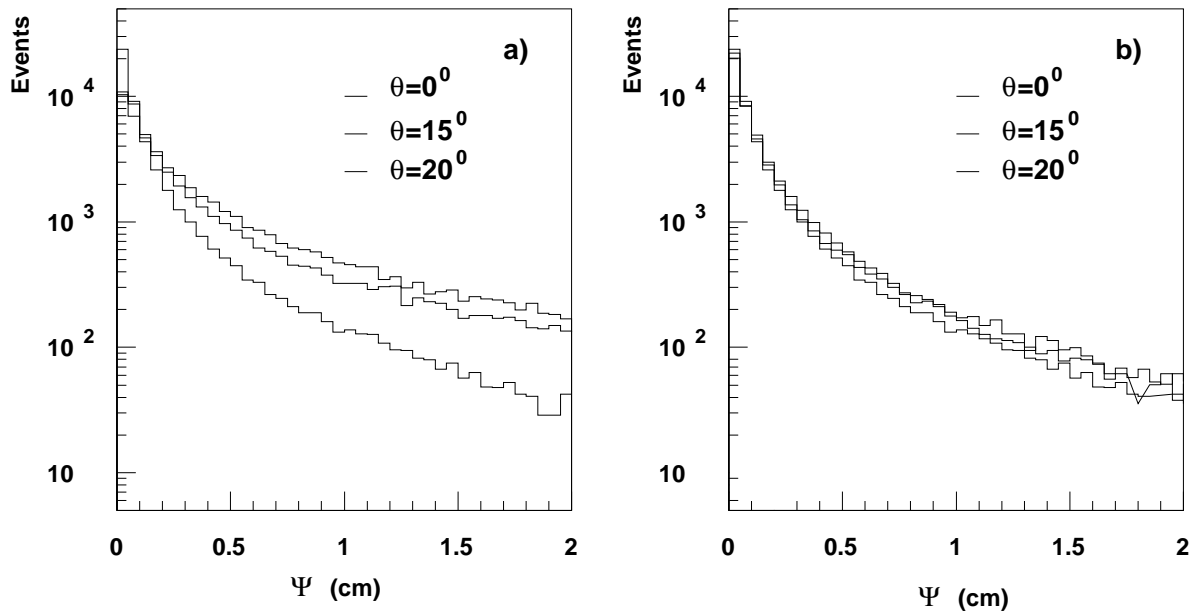


Figure 16: *Angular effects in* $\Psi$ *distributions for* $E = 5 GeV$: *a) for standard distances* $R_{ij}$ *and b) for corrected distances (see text).*

Because of the large interaction length $\lambda$ with respect to the cell size, the transverse radius of hadronic showers may extend over several blocks. As a consequence the angular dependence is expected to be less pronounced , compared to that of electromagnetic showers. Some attempts were made to take into account such a dependence simply by using corrected distances between the impact point and the cluster cells, as explained below.

The transverse distances $R_{ij}$ between the tower $(i, j)$ and the impact track of the particle were calculated with respect to a point inside the glass located half an interaction length along the track. As can be seen from the corresponding $\Psi$ distributions (figure 16) the angular dependence of $\Psi$ was much reduced. The resulting residual energy (figure 17) shows a weak dependence on angles of incidence up to $\theta = 20^0$.

The energy dependence observed for $\theta = 0^0$, described in section 6, is expected to become less evident when increasing the impact angle, since the hadronic shower has a larger effective transverse radius in this case and the probability of interaction increases with the path inside the glass. As can be seen from the comparison reported in figure 18a-b, for particle energies in the range $2 < E < 15\ GeV$, the results of the subtraction procedure do not depend significantly on the energy at $\theta = 15^0$. The $\Psi$ distributions (figure 18a) can be essentially superimposed and only a small increase in the residual energy is observed (figure 18b).
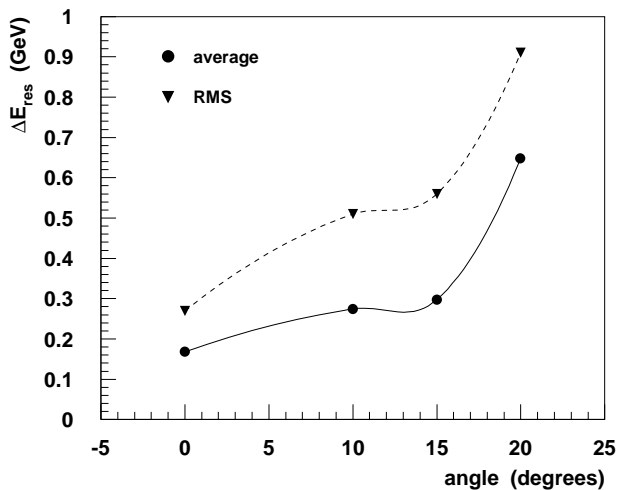


Figure 17: *Average and RMS values of the remaining energy in the calorimeter after hadron subtraction as a function of the angle of incidence for $E = 5\ GeV$ at P=0.05.*

## 10    Application to Neutrino Events

The methods described in the previous sections were applied to $\nu_\mu$ charged current events $(\nu_\mu CC)$ in order to check their performance in a neutrino environment. A sample of Monte Carlo $\nu_\mu CC$ events have been analyzed with the subtraction algorithm.

The distributions of the hadronic energy remaining in the calorimeter, $\Delta E_{res}$, after the subtraction procedure at probability levels $P=0.1$ and $0.01$ are shown in figure 19. The average residual energy depends on $P$ weakly: $\Delta E_{res}$=0.35 GeV at $P$=0.1 and $\Delta E_{res}$=0.23
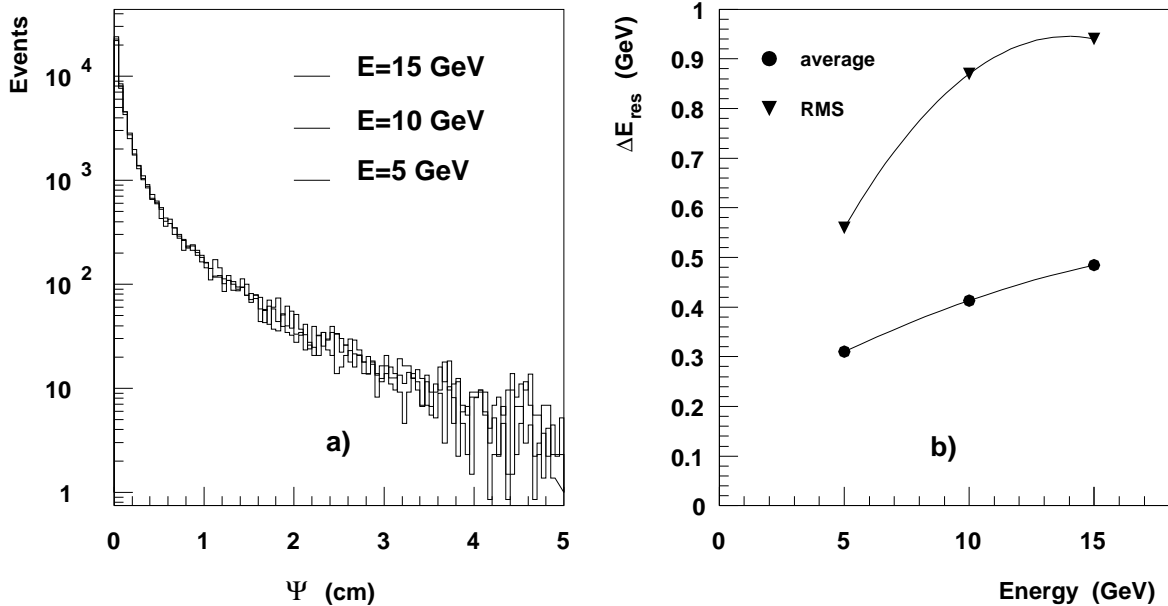
18

Figure 18: *Energy dependence for $E \leq 15$ GeV and $\theta = 15^0$ in MC data: a) $\Psi$ distributions and b) average and RMS values of the remaining energy in the calorimeter after subtraction procedure for $P = 0.05$. Corrected distances $R_{ij}$ were used.*

GeV at $P$=0.01. However, as one can see from figure 19 it affects significantly the tail in the distributions. The smaller the probability level the smaller the tail.

Since in the high energy neutrino collisions most of the particles are produced by hadronic jets, the photons may overlap with the nearby charged hadron tracks. The efficiency of photon reconstruction in the jets is affected by two effects. First, the probability that a photon overlaps with other tracks becomes large for more energetic photons since they are closer to the jet axis. Thus, the photon efficiency is lower compared to isolated case as given in the section 8.3. Second, in an ECAL area which is crowded by hadronic tracks the probability that more energy not belonging to a hadron will be associated to it is higher. The lower the probability level the less energy belonging to hadrons will be lost, but the more energy not belonging to it will be associated to it. This is illustrated by figures 20a,b where the average fractions of fake and lost photons versus their energies are shown for different probability levels for $\nu_\mu CC$ events. The dependence of these fractions on $P$ averaged over photons with energy more than 0.2 GeV is shown in figure 21.

The final choice of the probability level $P$ for the data analysis depends on the particular channel in which the oscillation signal is searched for.

## 11   Conclusions

We have presented results on fluctuations of the lateral shape of charged hadrons in a prototype of the NOMAD electromagnetic calorimeter. Both test beam results and Monte Carlo simulations show that the large event-to-event fluctuations of the lateral shape in hadronic showers make it difficult to identify and associate all hadronic energy deposited in the calorimeter to the incoming hadron track, simply using topological properties of the energy deposition with respect to the trajectory of the track. Some fraction of this energy could be misidentified, in particular in rare hadronic events with significant energy depositions at radii much larger than the ECAL cell size.
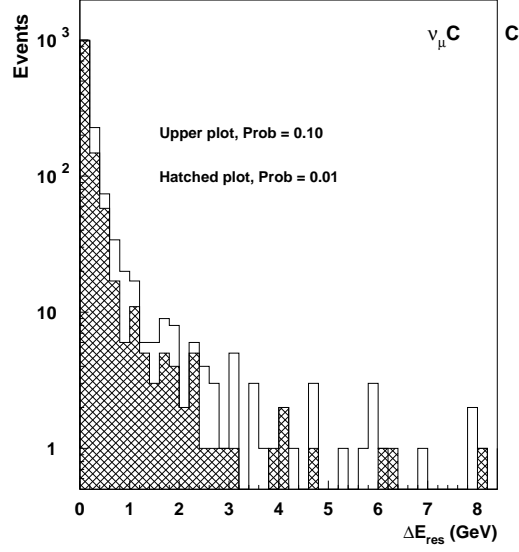
19

Figure 19: *Distributions of hadronic energy remaining in the calorimeter after the subtraction procedure at probability levels $P = 0.1$ and $0.01$ for $\nu_\mu CC$ events.*
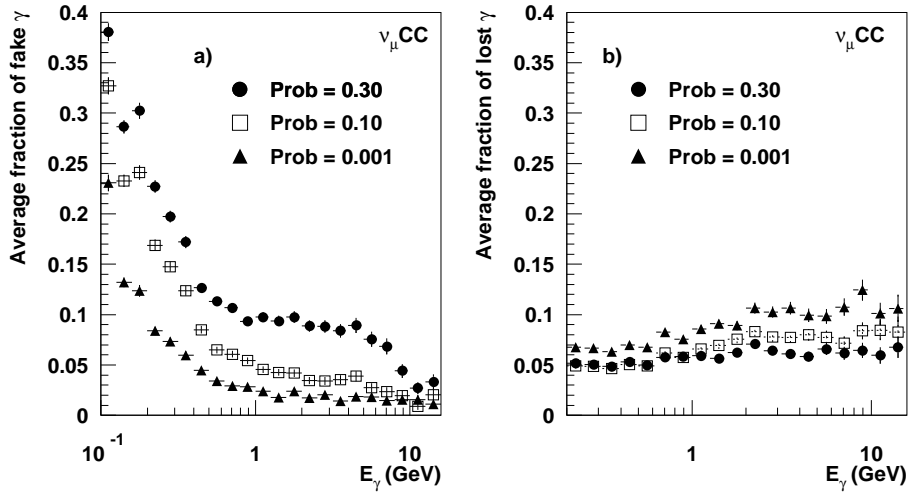


Figure 20: *Distributions of the average numbers of the a)fake and b)lost photons in the calorimeter as a function of their energy after the subtraction procedure at probability levels $P = 0.3$, $0.1$ and $0.001$ for $\nu_\mu CC$ events.*
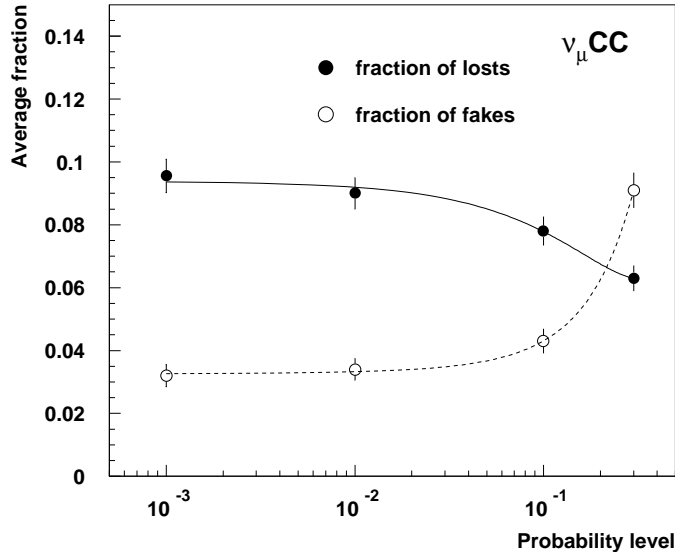
Figure 21: *Average fraction of fake and lost photons per $\nu_\mu CC$ event after hadron subtraction as a function of the probability level P. The curves are a polynomial fit to the data.*

A phenomenological method to describe these event-to-event fluctuations in terms of probability functions is developed. The well known problems related to the complexity of hadronic shower descriptions, in particular for nonzero incidence angles and large calorimeter cell size, were encountered. Nevertheless, the method is seen as an effective tool for the subtraction of the energy contribution due to charged hadrons in the NOMAD electromagnetic calorimeter. It also allows to evaluate the amount of hadronic energy remaining in the calorimeter after the subtraction procedure and, in particular, to estimate the probability for the rest of the energy in the ECAL to be reconstructed as fake neutral energy. The optimization of the efficiency for photon detection and signal-to-fake neutral energy background ratio both become possible by using a subtraction procedure with different probability cuts. We believe the approach described could be useful in all experimental conditions in which an accurate measurement of the energy deposited by charged hadrons in an electromagnetic calorimeter is needed.

The method also proved to be useful for identifying and unfolding overlapping showers. Our analysis shows that it is possible to separate particles entering the calorimeter at relatively small distances in space by analyzing the shape of the deposited energy. Two 5 $GeV$ pions, one of which considered as a neutral hadron, could be separated in more than 50% of the cases down to a distance of 6 $cm$. This distance increases to 20 $cm$ for 90% efficiency. A photon with energy greater than 3 $GeV$ overlapping a 15 $GeV$ pion can be separated with 90 % efficiency down to distances of 10 $cm$.

Test beam data on single-pion showers were found in general agreement with Monte Carlo simulations in the distributions of integral probability for energy deposition at a given radius. From the point of view of the analysis described the Monte Carlo correctly reproduces the experimental data and was successfully used to study the subtraction model in a large set of configurations. In particular, it was shown that the angular dependence of the hadronic shower development could be taken into account with simple

corrections. The shower analysis in terms of $A(f,R)$ and $P(\varepsilon,f,R)$ functions can then be adopted for angles of incidence up to $20^0$.

## 12  Acknowledgments

## References

[1] NOMAD proposal and addenda:
CERN-SPSLC/91-21, CERN-SPSLC/91-48, CERN-SPSLC/91-53,
CERN-SPSLC/93-19, CERN-SPSLC/94-21, CERN-SPSLC/94-28.

[2] NOMAD Collaboration, J.Altegoer et al., preprint CERN-PPE/97-059; to be published in *Nucl. Instr. Meth.*

[3] D.Autiero et al., *Nucl. Instr. Meth.* **A373** (1996) 358.

[4] D.Acosta et al., *Nucl. Instr. Meth.* **A316** (1992) 184.

[5] S.N.Gninenko, to be published in Proc. 7th Pisa Meeting on Advanced Detectors, La Biodola, Isola d'Elba, Italy, 1997.

[6] GEANT, CERN Program Library Long Writeup W5013, edition March 1994.